Journal of Membrane Science 698 (2024) 122538

Contents lists available at ScienceDirect

Journal of Membrane Science

journal homepage: www.elsevier.com/locate/memsci

Water content of ion-exchange membranes: Measurement technique and influence on the ion mobility

Alaaeldin A.E. Elozeiri [a], Rob G.H. Lammertink [b], Huub H.M. Rijnaarts [a], Jouke E. Dykstra [a,*]

[a] Environmental Technology, Wageningen University & Research, Bornse Weilanden 9, 6708 WG, Wageningen, the Netherlands
[b] Membrane Science and Technology, Faculty of Science and Technology (TNW), University of Twente, Drienerlolaan 5, 7522 NB, Enschede, the Netherlands

ARTICLE INFO

Keywords:
Water content
Ion mobility
Membrane tortuosity
Diffusion coefficient

ABSTRACT

Ion-exchange membranes (IEMs) are essential components of several electrochemical water technologies where they promote the transport of certain ionic species over others. A characteristic property of IEMs concerns their ionic charge density (ICD) which is a key parameter for modeling ion transport. In literature, significant variations in ICD for similar membranes are reported. We analyzed the sources of variations of this property and traced those back to the water content measurement. In this manuscript, we developed a new technique for measuring the water content, i.e., via stacking layers of membranes. This technique reduces the impact of the surface water film on the water content measurement. Using this technique, we measured the water content of CEMs at different counter-ion forms and analyzed the contribution of the ionic hydration shells inside the membrane. The relative change in the measured water content for the studied membranes at different counter-ions (K^+, Mg^{2+}, or Ca^{2+}) was below 23 % of the Na^+ value. Furthermore, we examined the relation between the water volume fraction and the membrane tortuosity, where we compared the theoretical predictions of ion mobility based on the Mackie and Meares theory to the values calculated based on the membrane resistance measurements.

1. Introduction

Ion-exchange membranes (IEMs) [1,2] form a key element in several electrochemical processes, such as electrodialysis, flow batteries, fuel cells, and electrolysis. Those membranes are characterized by their high ionic charge density, owing to charged groups that are fixed to the membrane polymer. The charge of those groups, whether positively or negatively, determines the selectivity of the membranes for either cations or anions [3,4]. For example, cation-exchange membranes (CEMs) have a high density of fixed anionic groups which favors the transport of cations while excluding anions.

IEMs swell differently depending on the salinity and composition of the solution in contact [5]. The water content, also called water uptake or swelling degree, WC [g H_2O/g dry polymer] [6,7], of IEMs influences ion transport due to its interdependence with membrane properties, such as its ionic charge density (ICD). The ionic charge density is defined either on the basis of (a) the water volume inside the membrane (Eq. 1a), or (b) the overall volume of the swollen membrane (Eq. 1b) [8]:

$$\mathrm{ICD_a\ [mol/L\ water\ sorbed]} = \frac{\mathrm{IEC}\cdot\rho_W}{\mathrm{WC}} \qquad \text{Eq. 1a}$$

$$\mathrm{ICD_b\ [mol/L\ swollen\ polymer]} = \mathrm{IEC}\cdot\rho_m \qquad \text{Eq. 1b}$$

$$\rho_m = \frac{m_{m,dry}}{A_m\cdot\delta_m} \qquad \text{Eq. 2}$$

where ρ_m [g dry polymer/mL swollen polymer] and ρ_W [g H_2O/mL H_2O] represent the membrane and water densities, respectively. The membrane wet thickness, dry mass, and wet surface area are expressed by δ_m [m], $m_{m,dry}$ [g dry polymer] and A_m [m^2 swollen polymer], respectively. Both Eqs. 1a and 1b depend on the ion-exchange capacity of the membrane, IEC [mmol/g dry polymer]. In this study, we discuss the error propagation and assumptions underlying each approach since both units can be adopted to describe the ion equilibria in membranes.

In Table 1, we summarize the measured values for two frequently reported membranes in literature: Selemion CMV and Neosepta CMX. Even for studies reporting similar values of IEC, there are still significant variations in the reported ICD due to the WC measurement. For example, some studies [9–14] measured similar values for IEC (1.62 – 1.69

* Corresponding author.
E-mail address: jouke.dykstra@wur.nl (J.E. Dykstra).

https://doi.org/10.1016/j.memsci.2024.122538
Received 9 October 2023; Received in revised form 24 January 2024; Accepted 4 February 2024
Available online 14 February 2024

mmol/g dry IEM Neosepta CMX), while the ionic charge density varied between 3.9 and 9.0 mol/L water sorbed. Besides, the WC values, summarized in Table 1, were reported with an inconsistent number of significant figures (2 – 4 significant figures) without a justification regarding the measurement uncertainty.

The membrane water content (WC, also called water uptake or swelling degree) is calculated based on its wet and dry mass, both measured gravimetrically.

$$WC = \frac{m_{m,wet} - m_{m,dry}}{m_{m,dry}} \quad \text{Eq. 3}$$

where m_m is the mass of the membrane sample. The subscripts, wet and dry, refer to a membrane in wet (swollen) and dry conditions, respectively. Measuring the mass of a wet membrane is challenging. Once the membrane is taken out of the solution, water droplets adhere to its surface. To remove surface water, different gravimetric techniques were reported: via dry tissue [15,16], paper [9,17], or wipe [6,8,18]. Furthermore, Bass and Freger [19] calculated the water content of small square pieces of Nafion and beads of Dowex based on optical measurement of the sample area. The measurement is made without taking the samples out of the solution. However, this method assumes isotropic swelling of the swollen polymer. As we elaborate later, this assumption does not necessarily reflect the swelling of commercial IEMs; as they usually contain a reinforcement mesh that hampers isotropic swelling.

In this study, we aim to standardize the membrane water content measurements. We noticed significant variations in the results based on how the excess water on the membrane surface is removed. To overcome such deviations, we propose a membrane stacking technique. We further investigate the influence of the counter-ions inside the membrane on its water content and analyze the contribution of the hydration shell of ions. In addition, we highlight the relation between the water fraction of the membrane and its ion mobility.

2. Materials and methods

We studied six types of CEMs: Selemion CMTE and CMVN (Asahi Glass Co., Japan), Fumasep FKS-PET-130 and FKD-PK-75 (Fumatech BWT GmbH, Germany), in addition to Fujifilm CEM type-10 and type-12 (Fujifilm Manufacturing Europe BV., The Netherlands). Sodium chloride (NaCl) was purchased from VWR Chemicals. Sodium sulfate (Na_2SO_4), potassium chloride (KCl), magnesium chloride ($MgCl_2$), calcium chloride ($CaCl_2$), and hydrochloric acid (HCl 37 %) were purchased from Sigma-Aldrich. Solutions were prepared using Milli-Q water (Millipore). All experiments were performed at 19 – 22 °C.

2.1. Membrane thickness and water content measurements

Five samples (~3 × 3 cm^2 each) of each membrane type were initially used for water content measurements. The membranes are first equilibrated in a solution of 0.5 M NaCl overnight where the solution was refreshed once. We removed the excess water on the membrane surface via one of the following methods, and immediately measured the wet membrane mass gravimetrically using an analytical balance (Mettler Toledo, precision: 10^{-4} g):

(A) Shaking the membrane in air three times
(B) Drying membrane surface with a thick tissue (thickness 160 μm)
(C) Drying membrane surface with a thin tissue (thickness 100 μm, lower absorption capacity)
(D) Drying membrane surface with a dry paper (thickness 103 μm)

Methods (A – D) were performed on the same samples where the samples were re-equilibrated in the solution before each measurement. After measuring the wet sample mass for all the methods, the samples were dried to calculate the water content according to Eq. 3 (the drying procedure is described later). We noticed significant variations in the membrane WC results depending on the way of removing the surface water (Fig. 5). We then cut eight new samples (~3 × 3 cm^2 each) of each membrane material and equilibrated them at 0.5 M NaCl. To eliminate the influence of the surface water film on the calculated water content, we stacked eight layers of the membrane on a plastic support (Fig. 1). After adding each layer to the membrane pile, the top surface is rubbed to remove any water that might be trapped between the layers. A plastic frame was mounted on the top of the stack with four plastic screws to hold the stack together and to keep the membrane layers flat, aligned, and stationary (Figure SI- 3). Otherwise, some types of IEMs tend to curl or corrugate, which can overestimate the membrane water content.

Table 1
Reported ion-exchange capacity (IEC) and water content (WC) values for Selemion CMV and Neosepta CMX membranes in literature. (*): the values are presented in this table with the same number of significant figures as reported in the references. (**): the ionic charge density in this table is calculated based on Eq. (1a), assuming a water density of 1 g/mL. [a] the measurement method for IEC was not reported. [b] the author used a different procedure than the common acid/base titration method for IEC measurement. n.r. not reported.

Membrane	IEC (*) [mmol/g dry polymer]	WC (*) [g H_2O/g dry polymer]	ICD (**) [mol/L H_2O sorbed]	the membrane was equilibrated in	Surface water removed with	To obtain the dry mass, the membrane was dried at	Ref.
Selemion CMV	1.89	0.23	8.2	4 M NaCl	laboratory wipe	65 °C for 48 h	[6]
	1.95	0.19 – 0.21	9.3 – 10.3	0 – 1 M NaCl	wipe	40 °C for 48 h	[7, 20]
	2.01	0.20	10.1	n.r.	blotting paper	50 °C for 48 h	[9]
	2.01	0.293	6.9	1 M NaCl	wipe	35 °C for 24 h	[21]
	2.01 [9]	0.296	6.8	n.r.	n.r.	n.r.	[10]
	2.08	0.266	7.8	n.r.	n.r.	40 °C for 48 h	[22]
	2.3[a]	0.3709	6.2	n.r.	n.r.	n.r.	[11]
Neosepta CMX	1.5–1.8	0.25 – 0.30	5.0–7.2	n.r.	n.r.	n.r.	[23]
	1.57	0.258	6.1	n.r.	n.r.	40 °C for 48 h	[22]
	1.62	0.18	9.0	n. r.	blotting paper	50 °C for 48 h	[9]
	1.62 [9]	0.222	7.3	n.r.	n.r.	n.r.	[10]
	1.65[a]	0.275	6.0	n.r.	n.r.	n.r.	[11]
	1.66 ± 0.06	0.220 ± 0.003	7.5	n.r.	n.r.	n.r.	[12]
	1.68 ± 0.09	0.40 – 0.43	3.9 – 4.2	0.01 – 1 M NaCl	wipe	vacuum oven for 48 h at room temperature	[13]
	1.69[b]	0.30	5.6	n.r.	n.r.	Dried over MgSO4 for 24 h	[14]
	1.77	0.22	8.0	4 M NaCl	laboratory wipe	65 °C for 48 h	[6]
	2.18[b]	0.336	6.5	1 M NaCl	n.r.	40 °C vacuum oven for 24 h	[24]
	–	0.32	–	n.r.	n.r.	n.r.	[25]

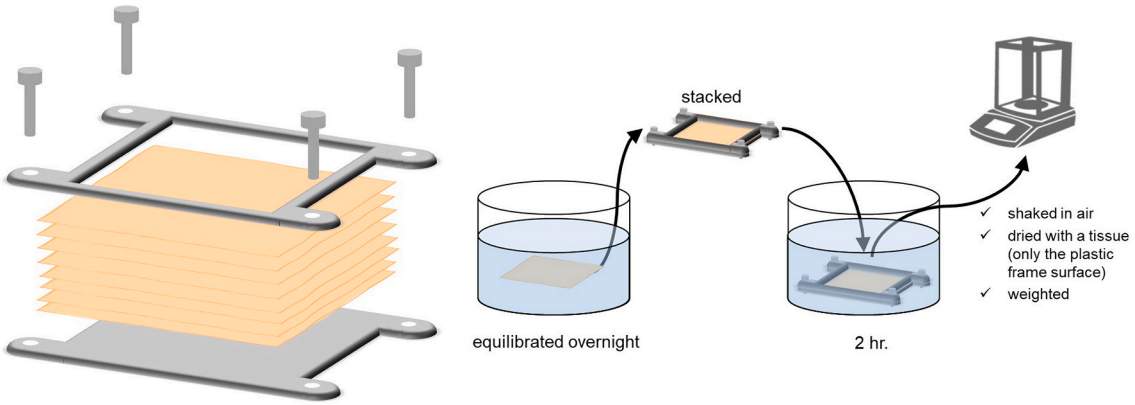

Fig. 1. Membrane stacking measurement.

Table 2
Solutions used to exchange the membrane counter-ion form.

counter-ions exchanged		Solution used	Total duration [h]	Solution was refreshed
from	to			
Na^+	K^+	0.2 M KCl	2.5	twice
K^+	Mg^{2+}	0.1 M $MgCl_2$	3	twice
Mg^{2+}	Ca^{2+}	0.01 M $CaCl_2$	3	twice
Ca^{2+}	H^+	1 M HCl	18	once

After the screws are tightened, the membrane sheets cannot move/shift during the measurement. The four screws were tightened to the same degree. Overtightening the stack was avoided to prevent the deformation of the plastic support material. The plastic support was 3D printed with acrylonitrile butadiene styrene material (Ultimaker ABS). While the bottom support is closed, the top frame is open to give some flexibility for the membranes to swell or shrink.

After equilibrating in solution for at least 2 h, the stack was removed from the solution with a tweezer and shaken three times in air. During shaking the stack, the open frame was pointed downwards. A tissue was used to properly remove any water droplets on the bottom and top plastic frames as well as near the screws. Afterward, the wet stack mass was measured gravimetrically. Touching any of the membrane material with the tissue must be avoided. This ensures that the tissue does not withdraw random amounts of the water inside the membrane.

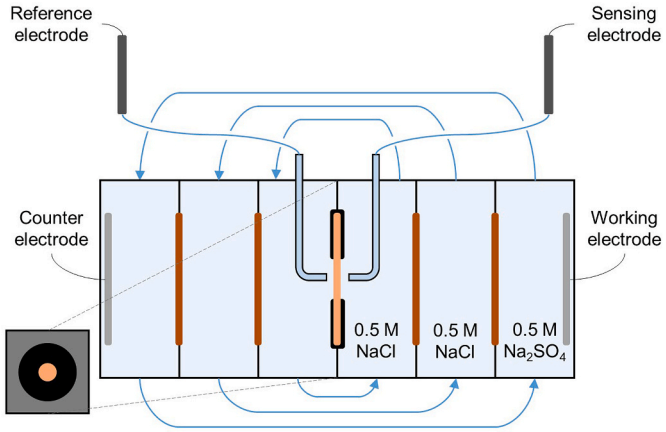

Fig. 2. The six-compartment cell used for direct and alternating current measurements based on a four-electrodes configuration. Three solutions are recirculated through the cell. The middle membrane (light orange) is the membrane under investigation. The other four membranes (dark orange) are auxiliary membranes used to separate the different solutions.

Moreover, the shaking and the drying of the plastic parts were done consistently to have a constant contribution of the water film on the top membrane surface throughout all measurements.

To this point, we weighed the stack of 8 membrane layers. Subsequently, we removed the top layer from the stack and returned the stack to the solution for 10 – 15 min before the next stack (7 layers) measurement. Carrying on with this procedure, we obtained 8 measurements of the wet stack mass for each membrane material. Moreover, we kept the order of samples while removing each layer; so that we measure the dry mass of each layer and correlate it accurately. As we follow the same technique in each measurement, we assumed constant contributions to each set of measurements (b_0): the mass of the plastic support, screws, and the water film on the top membrane surface. Therefore, the total measured mass of the wet stack, $m_{stack,k}$, can be linearly correlated to the total dry membrane mass as follows

$$y_k = b_1 \cdot x_k + b_0 \quad \text{Eq. 4}$$

$$y_k = m_{stack,k} \quad \text{Eq. 5}$$

$$x_k = \sum_{i=1}^{k} m_{m,dry,i}^{X\ form} \quad \text{Eq. 6}$$

$$b_1 = 1 + WC \quad \text{Eq. 7}$$

where $m_{stack,k}$ is the total mass of the wet stack including (k) layers of membranes, $m_{m,dry,i}^{X\ form}$ is the dry mass of membrane sample (i), and the superscript (X) refers to the type of counter-ions (according to Eq. 18). The subscripts, i and k, refer to the sample order and the number of membrane layers in the wet stack, respectively. We calculated the regression coefficients (b_1 and b_0) via the least squares method [26–28] as follows

$$b_1 = \frac{\sum_{k=1}^{N}(x_k - \bar{x})(y_k - \bar{y})}{\sum_{k=1}^{N}(x_k - \bar{x})^2} \quad \text{Eq. 8}$$

$$b_0 = \bar{y} - b_1 \cdot \bar{x} \quad \text{Eq. 9}$$

where $\bar{x}$ and $\bar{y}$ are the means of the x and y values, respectively. The variance of y about the regression line was estimated based on the residual variance (s^2) [27,28]

$$s^2 = \frac{\sum_{k=1}^{N}(y_k - \bar{y})^2 - b_1^2 \cdot \sum_{k=1}^{N}(x_k - \bar{x})^2}{N - 2} \quad \text{Eq. 10}$$

where N is the number of data points (N = 8). The denominator represents the degrees of freedom, where two degrees of freedom are used for

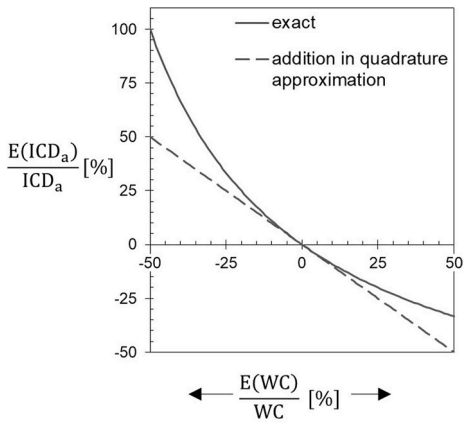

Fig. 3. Theoretical error propagation from the water content (WC) measurement to the ionic charge density (ICD) where the relative error in the ICD_a [mol/L water sorbed] is plotted as function of the relative error in the WC parameter. The solid line refers to the exact error propagation based on Eq. 25a, while the dashed line represents the approximated error using Eq. 27. Similar trend can be plotted for the error propagation from the membrane thickness measurement to the ICD calculated via Eq. (1b).

the determination of the two regression coefficients. We evaluated the standard error [27,28] in the regression coefficients via

$$SE_{b_1} = \sqrt{\frac{s^2}{\sum_{k=1}^{N}(x_k - \bar{x})^2}} \quad \text{Eq. 11}$$

$$SE_{b_0} = s \cdot \sqrt{\frac{1}{N} + \frac{\bar{x}^2}{\sum_{k=1}^{N}(x_k - \bar{x})^2}} \quad \text{Eq. 12}$$

Using the (two-tailed) Student's t-distribution (t_{N-2}) value for a 90 % confidence level and (N-2) degrees of freedom, we estimated the confidence interval (CI) [27,28] for the WC as

$$CI_{WC} = WC \pm t_{N-2} \cdot SE_{b_1} \quad \text{Eq. 13}$$

Using this method, the same samples of each membrane material and stacks were used to measure the water content at different salinities: 0.01, 0.1, 0.5, and 1 M NaCl. The membranes were always equilibrated in the solution of interest overnight, during which the solution was renewed at least once.

The length and width of the wet (equilibrated in 0.5 M NaCl) and dry membrane samples were measured with a digital caliper (resolution: 0.01 mm). Furthermore, we obtained the wet and dry membrane thicknesses using a digital micrometer (Micromar, Mahr GmbH, resolution: 1 μm).

Table 3
Membrane thickness and area density for different commercial CEMs. The ± values for the surface area density represent the standard deviation based on 8 measurements.

membrane	reinforcement	thickness		surface area density	
		dry	wet		
		[μm]	[μm]	[g dry polymer/m^2 wet IEM]	
				avg	+/−
CMTE	unkown	219 – 227	250 – 270	195	3
CMVN	unkown	88 – 95	97 – 103	107	2
FKS	Polyester [37]	146 – 152	138 – 150	119	2
FKD	PEEK [37]	90 – 97	103 – 110	76	1
Fuji-T10	Polyolefin [38]	115 – 125	125 – 155	84	2
Fuji-T12	Polyolefin [38]	118 – 126	119 – 132	93	1

2.2. Counter-ion exchange

We exchanged the counter-ions inside the membrane samples to K^+, Mg^{2+}, and Ca^{2+}. After each exchange, the samples were equilibrated in a 10 mM solution of the corresponding chloride salt (i.e., KCl, $MgCl_2$, or $CaCl_2$). The water content of the membrane was measured following the same membrane stacking technique, described earlier. For each membrane material, we monitored the exchange of counter-ions in three samples.

The membrane samples (initially in Na^+ form) were firstly soaked in demi water for 2 h (with stirring and replacing the water 3 times); to desorb excess/mobile ions from the membrane. Afterward, the counter-ions of the membrane were replaced by K^+ via soaking in a 0.2 M KCl solution for a total duration of 2.5 h (with stirring and refreshing the solution twice). The three solutions were combined and the concentration of the desorbed Na^+ was measured using inductively coupled plasma - optical emission spectrometry (ICP-OES). The conversion percentage was calculated via

$$\text{Conversion} = \frac{V_s \cdot (C_{Na,after} - C_{Na,before}) \cdot z_{Na}}{m_{m,dry} \cdot IEC} \quad \text{Eq. 14}$$

where V_s is the collected solution volume, and z is the ion valence. The subscripts "after" and "before" refer to the KCl solution after and before the exchange step, respectively. Similarly, the samples were also exchanged with other ions by soaking the samples in the relevant solutions as summarized in Table 2.

2.3. Ion-exchange capacity (IEC)

We measured the IEC of CEMs based on the acid/base titration method [6,9,29,30]. Small pieces of CEM (~0.5 g wet) were brought to H^+ form by submerging the membrane in 200 mL of 1 M HCl solution overnight with gentle stirring. The solution was renewed and stirred for one more hour. The membranes were then soaked in demi water for 2 h (with stirring and replacing the water 3 times) to desorb excess/mobile ions from the membrane. Afterward, the membranes were transferred to a 50 mL solution of 2 M NaCl for 3 h where the solution was renewed twice. The three solutions were combined and titrated versus a NaOH solution of known concentration with an automatic titrator (Titrando, Metrohm). We measured the volume consumed to reach the equivalent point V_{NaOH}. Lastly, the membrane dry mass was measured as explained in the next section. The IEC was calculated using

$$IEC = \frac{V_{NaOH} \cdot C_{NaOH}}{m_{m,dry}} \quad \text{Eq. 15}$$

where V_{NaOH} is the volume of NaOH solution required to reach the

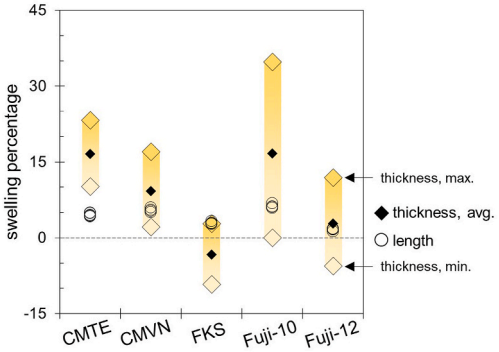

Fig. 4. Swelling percentage of the membrane along its thickness as well as its length. The swelling of the membrane length is marked with open circles (6 – 8 measurements per membrane material). The average thickness swelling is marked by black solid diamonds.

Table 4
Ion-exchange capacity (IEC) and ionic-charge density (ICD) of different commercial CEMs. The ± values for the IEC represent the standard deviation in 3 – 6 measurements. The ± values for the ICD represent the propagated errors according to the addition in quadrature approach (Methods section). For each membrane, the values, based on this study, are presented in the first row, and the values, retrieved from literature, are in the subsequent rows.

membrane	IEC	ICD	
		via Eq. 1a	via Eq. 1b
	[mmol/g dry polymer]	[mol/L water sorbed]	[mol/L swollen polymer]
CMTE	2.21 ± 0.09	3.8 ± 0.3	1.7 ± 0.1
CMVN	1.40 ± 0.04	3.7 ± 0.6	1.50 ± 0.07
	1.40 ± 0.02 [39]	7.7 ± 0.2 [39]	1.54 ± 0.02 [39]
	1.51 ± 0.01 [40]		
FKS	0.91 ± 0.01	2.0 ± 0.4	0.75 ± 0.03
	1.02 ± 0.03 [40]		
	1.0 [41]		
	0.8 – 1.2 [37]		
FKD	1.29 ± 0.04	1.59 ± 0.06	0.92 ± 0.04
	1.14 [9]		
	1.2 – 1.4 [37]		
Fuji-T10	2.45 ± 0.03	2.5 ± 0.2	1.5 ± 0.2
	2.74 ± 0.15 [39]	6.7 ± 0.4 [39]	1.69 ± 0.09 [39]
	2.12 ± 0.05 [17]		
Fuji-T12	1.46 ± 0.01	2.0 ± 0.2	1.08 ± 0.06
	1.55 ± 0.07 [39]	5.5 ± 0.3 [39]	1.15 ± 0.05 [39]

equivalence point, and C_{NaOH} is the NaOH concentration.

2.4. Membrane dry mass

The membrane samples were first converted to Na^+ form and then soaked in demi water for 2 h to wash out the excess mobile salt from the membrane, where the solution was refreshed twice. Afterward, the samples were left to dry at ambient laboratory conditions for 2 days, followed by an additional 10 h at N_2 atmosphere, and 2 h in a drying oven at 105 °C to ensure full drying. The samples were left to cool down inside a desiccator for 1.5 h where silica gel granules (Merck) were used as a drying agent. The dry sample mass was directly recorded once taken out of the desiccator. In the Supporting Info, SI-2, we further discuss the drying procedure and the influence of the dry mass measurement uncertainty on the WC and ICD calculations. For accurate measurement of the membrane dry mass, the samples should be exposed to a temperature above the boiling point of the water, yet stay below the thermal degradation limits of the polymer [31]. Moreover, an extended heating duration should be avoided as it promotes the oxidation of the membrane polymer.

As discussed earlier, the ICD can be calculated using the membrane density ρ_m [g dry polymer/mL swollen polymer] and IEC (Eq. 1b). The membrane density (Eq. 2) is calculated based on the dimensions of the membrane sample (i.e., width, length, and thickness) as well as its dry mass. To clarify the uncertainty in the membrane thickness measurement relative to the other parameters in Eq. 2, we formulate the membrane density, ρ_m [g dry polymer/mL swollen polymer], as follows

$$\rho_m = \frac{a_m}{\delta_m} \quad \text{Eq. 16}$$

$$a_m^{\text{Na form}} = \frac{m_{m,dry}^{\text{Na form}}}{A_m} \quad \text{Eq. 17}$$

where a_m [g dry polymer/m^2 swollen polymer] is the surface area density of membrane material, $m_{m,dry}^{\text{Na form}}$ [g] is the dry mass of the membrane sample having Na^+ as counter-ions, and A_m [m^2 swollen polymer] is the surface area of the wet membrane sample (equilibrated at 0.5 M NaCl).

The counter-ions inside the IEM contribute significantly to the dry membrane mass. For example, the Na^+ counter-ions account for 5 % of CMTE membrane's dry mass when it is fully exchanged in this form. For the stacking measurements, we used the same samples to measure the membrane water content at different counter-ion forms, but the samples were dried eventually in Na^+ form. Therefore, it is important to account for the accompanied change in the membrane dry mass to avoid inaccurate trends in water content calculations. The dry mass of a membrane sample where the counter-ions are X, $m_{m,dry}^{\text{X form}}$, is calculated as follows

$$m_{m,dry}^{\text{X form}} = m_{m,dry}^{\text{Na form}} \cdot \left(1 + IEC \cdot \left(\frac{M_X}{z_X} - \frac{M_{Na}}{z_{Na}}\right) \cdot 10^{-3}\right) \quad \text{Eq. 18}$$

where M_{Na} [g/mol] is the molar mass of Na^+ ions.

2.5. Membrane resistance

The membrane resistance was measured using a 6-compartment cell [9,32,33] (EMI Twente, The Netherlands) with circular platinum-coated titanium electrodes as cathode and anode (Fig. 2). To eliminate the influence of the working and counter electrodes on the measurements, we used a four-electrodes configuration where Ag/AgCl reference electrodes were connected to Haber–Luggin capillaries via a 3 M KCl solution. Moreover, the 6-compartment cell was placed in a Faraday cage to minimize the background electromagnetic noise. Three solutions were recirculated at 0.25 – 0.3 L/min through the cell and heat exchangers to keep the temperature at 20 °C (±1). To keep the solutions separated, four Selemion CMTE sheets were used as auxiliary membranes between the outer compartments. The membrane of interest was placed between the middle compartments in contact with a 0.5 M NaCl solution. The investigated membrane was sandwiched between area reducer rings (250 μm) in order to magnify its resistance relative to the solution resistance, and consequently, reduce the measurement error. The active membrane area was 5.4 ± 0.1 cm^2.

Direct current (DC) and alternating current (AC) were generated via a potentiostat (Ivium Technologies, The Netherlands). We analyzed the membrane resistance via DC followed by AC, each in triplicates. Before and after measuring the membrane resistance, we measured the (blank) solution resistance twice. At the blank runs, we inserted the area reducer ring without any membrane between the middle compartments. For DC measurement, a linear potential sweep between 0 and 0.2 V was performed using steps of 3 mV (Figure SI- 5b). The data of the linear ohmic part of the iV curve was used to calculate the resistance via linear fitting similar to the fitting approach introduced earlier for the stacking measurements (Eqs. 8–13). Moreover, the uncertainty in the calculated DC resistance (R^{DC}) was calculated based on a 90 % confidence level.

For electrochemical impedance spectroscopy (EIS) measurement, we applied AC sine waves of amplitude 10 mA at open circuit voltage and scanned the frequencies from 10^5 to 0.1 Hz. Długołęcki et al. [34] explained the equivalent circuit for the membrane impedance and measured the membrane response at lower frequencies (down to 10^{-3} Hz) and more dilute solutions (17 mM NaCl). For our measurements (at 0.5 M NaCl), the response in the frequency range of 500 – 1 Hz is purely resistive with negligible phase shift (Figure SI- 5a). Therefore, we used the average of the real impedances in this range as the system resistance. Moreover, the uncertainty in the AC measurements is based on the standard deviation of the data.

The membrane resistance (r_m) is the difference between the blank (solution only) and the combined (membrane + solution) resistance measurements.

$$r_m = r_{m+s} - r_s \quad \text{Eq. 19}$$

where r [Ω] is the system resistance. The subscripts "m" and "s" refer to the membrane and the solution respectively. The uncertainty/error in the membrane resistance E(r_m) is estimated as the summation of errors in both the blank and the combined (membrane + solution) resistance

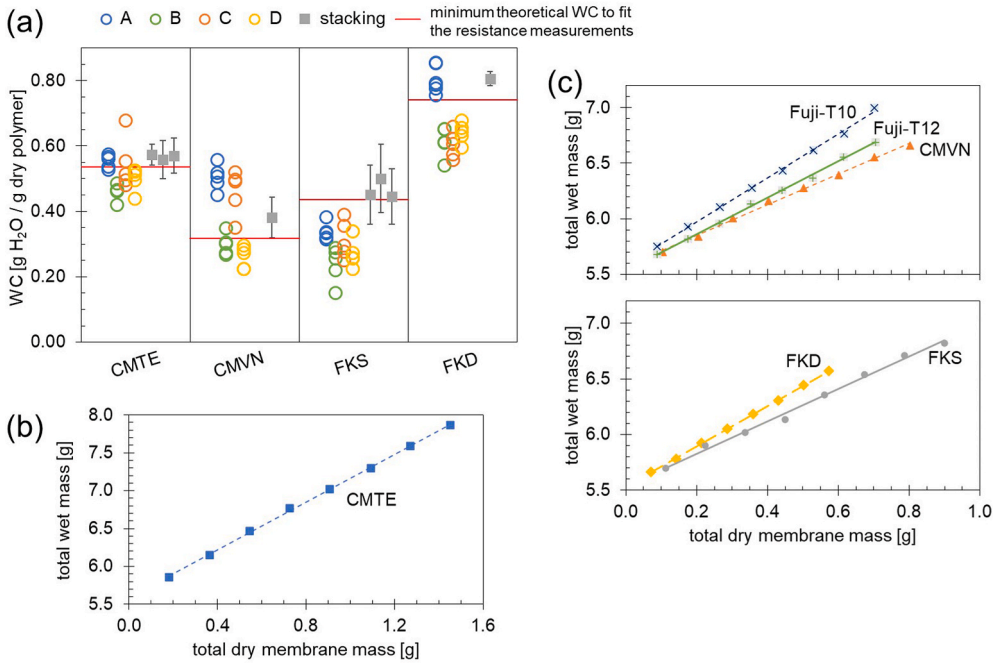

Fig. 5. (a) Measured water content (WC) at 0.5 M NaCl for four commercial CEMs using different methods to remove the surface water. Letters, A – D, represent the single membrane measurement methods as explained in the Materials and Methods section, where 5 measurements were performed for each method and each membrane. "Stacking" refers to the membrane stacking method. The error bars for the stacking method reflect a 90 % confidence level. The red lines refer to the minimum WC that corresponds to the measured membrane resistance as per the theoretical framework of Mackie and Meares (details are discussed in the next sections). (b, c) Linear fitting of the water content measurements (at 0.5 M NaCl) via the stacking method. The markers represent the measured values, while the dashed line is the linear fit.

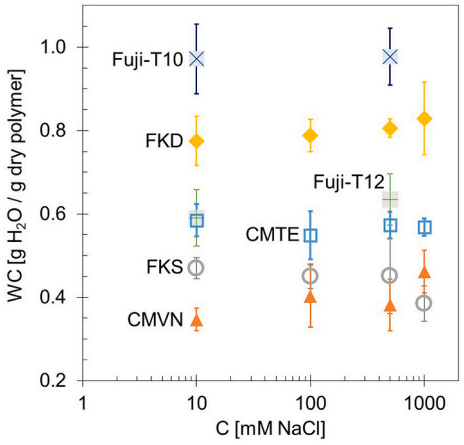

Fig. 6. Effect of the NaCl concentration of the external solution on the membrane water content based on the stacking method. The error bars represent a 90 % confidence level.

measurements as follows

$$E(r_m) = E(r_{m+s}) + E(r_s) \quad \text{Eq. 20}$$

The membrane-area resistance (R_m [$\Omega.cm^2$]) is calculated as follows

$$R_m = A_m \cdot (r_{m+s} - r_s) \quad \text{Eq. 21}$$

where A_m [cm^2] is the active membrane area. Furthermore, the membrane-area resistance (R_m) translates to a membrane-specific resistance ($R_{m,specific}$) and conductivity (κ_m) [35] as follows

$$R_{m,specific} = \frac{R_m}{\delta_m} \quad \text{Eq. 22}$$

$$\kappa_m = \frac{1}{R_{m,specific}} \quad \text{Eq. 23}$$

2.6. Error propagation analysis

Earlier, we explained how we estimate the error or uncertainty in the measurement, e.g., the WC measurement. In this sub-section, we clarify how to estimate the combined error propagation from multiple parameters to one parameter, e.g., ICD.

(a) One-to-one

It is useful to first examine the propagation of an arbitrary error from one parameter to another, specifically to the ionic charge density. As introduced earlier, the ICD can be calculated using either Eq. 1a or 1b. For the former approach (Eq. 1a), we calculate the theoretical error propagation from the water content measurement to the ICD_a as follows

$$ICD_a + E(ICD_a) = \frac{IEC \cdot \rho_W}{WC + E(WC)} \quad \text{Eq. 24}$$

$$\frac{E(ICD_a)}{ICD_a} = \frac{1}{1 + \frac{E(WC)}{WC}} - 1 \quad \text{Eq. 25a}$$

Table 5
Exchange of counter-ions inside the membranes (rounded values).

exchanged		solution used	conversion [%]			
from	to		CMTE	CMVN	FKS	FKD
Na	K	0.2 M KCl	90	100	90	85
K	Mg	0.1 M $MgCl_2$	100	100	90	95
Mg	Ca	0.01 M $CaCl_2$	95	100	100	100
Ca	H	1 M HCl	100	100	90	95

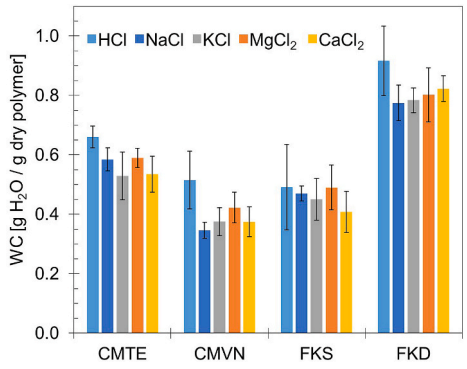

Fig. 7. Membrane water content at different counter-ion forms, where the samples were equilibrated in 10 mM of the corresponding (X)Cl_y solution. The error bars represent a 90 % confidence level.

where E is the error or uncertainty in the measured or calculated parameter. Similarly, the error propagation from the membrane thickness measurement to the ICD_b can be calculated as follows

$$\frac{E(ICD_b)}{ICD_b} = \frac{1}{1+\frac{E(\delta_m)}{\delta_m}} - 1 \qquad \text{Eq. 25b}$$

In both cases (Eqs. 25a and 25b), the relative error in the ICD is not linear in response to the relative error in the membrane thickness, or the membrane WC measurements (solid line in Fig. 3). Furthermore, underestimating the membrane thickness or WC leads to higher relative errors in the ICD compared to overestimating.

(b) Multiple-to-one

Secondly, we consider the propagation of multiple uncertainties to one parameter, e.g., the propagation of the WC, and IEC measurements uncertainties to the ICD. It is unlikely that the errors in each of the WC and IEC will accumulate in the same direction to either maximize or minimize the ICD. It is also unlikely for those errors to perfectly cancel each other. Taylor [36] treated this statistical problem and suggested a general formula to calculate the uncertainty in a variable, e.g., q, which is a function of parameters: A, …, Z measured with uncertainties of E(A), …, E(Z), respectively. We reformulate his general equation ("addition in quadrature", equation 3.47 in Ref. [36]) as follows

$$E(q) = \sqrt{\left(E(A)\cdot\frac{\partial q}{\partial A}\right)^2 + \ldots + \left(E(Z)\cdot\frac{\partial q}{\partial Z}\right)^2} \qquad \text{Eq. 26}$$

where $\partial q/\partial A$ is the partial derivative of q with respect to A. This equation is applicable when the uncertainties in A, .., and Z are independent and random [36]. For example, the measurement of the IEC is independent of that of the WC or the membrane thickness. However, that is not necessarily the case for the measurements of the combined membrane and solution resistance (r_{m+s}) versus the blank (solution only, r_s) resistance since those measurements were performed consequently using the same procedure and equipment. Therefore, the uncertainty in the membrane resistance ($E(r_m)$) was estimated as a simple summation of the uncertainties in each of the combined (membrane + solution) and the blank measurements (Eq. 20).

The addition in quadrature is an estimation that simplifies the complex problem of multi-error propagation. Nevertheless, an underlying assumption [36] is that the uncertainties in A, …, and Z are small. To examine the accuracy of Eq. 26, we derive the special case of the error propagation from the WC to the ICD as follows

$$\frac{E(ICD_a)}{ICD} = \frac{-E(WC)}{WC} \qquad \text{Eq. 27}$$

Table 6
Ion properties at 25 °C: molar mass, Gibbs free energies of hydration [68], ionic crystal radii [69], and hydrated radii in aqueous solution [62]. The last two columns present the calculated water volume associated with the ionic hydration shell and the hydration number in a CEM, respectively. n.a.: not applicable.

Ion	Molar mass [g/mol]	$-\Delta_{hyd}G°$ [kJ/mol]	Crystal radius [A°]	Hydrated radius [A°]	$V^{eq.}_{hyd.,i}$ [mL H_2O/mol eq.]	$\lambda^{m}_{hyd.}$ [mol H_2O/mol eq.]
Na^+	23.0	365	0.95	3.58	114	12.7
K^+	39.1	295	1.33	3.31	86	10.9
Mg^{2+}	24.3	1830	0.65	4.28	99	11.7
Ca^{2+}	40.1	1505	0.99	4.12	87	11.0
Cl^-	35.5	340	1.81	3.32	77	n.a.

We ignored the uncertainty of IEC in Eq. 27 only for the sake of a theoretical comparison with Eq. 25a. This approximation was plotted against the exact solution (Fig. 3). As a rule of thumb, the "addition in quadrature" (Eq. 26) provides reasonable error estimations when the relative uncertainty in the measurements is below 10 %, which is generally the case for the measurements performed in this study. In the results section, we present the uncertainty in the ICD based on the addition in quadrature equation as follows

$$E(ICD_a) = ICD_a\cdot\sqrt{\left(\frac{E(IEC)}{IEC}\right)^2 + \left(\frac{E(WC)}{WC}\right)^2} \qquad \text{Eq. 28}$$

$$E(ICD_b) = ICD_b\cdot\sqrt{\left(\frac{E(IEC)}{IEC}\right)^2 + \left(\frac{E(\lambda_m)}{\lambda_m}\right)^2 + \left(\frac{E(\delta_m)}{\delta_m}\right)^2} \qquad \text{Eq. 29}$$

Moreover, the uncertainty in the membrane-area resistance ($E(R_m)$) is calculated as follows

$$E(R_m) = R_m\cdot\sqrt{\left(\frac{E(A_m)}{A_m}\right)^2 + \left(\frac{E(r_m)}{r_m}\right)^2} \qquad \text{Eq. 30}$$

3. Results

3.1. Membrane thickness and IEC

Using a desk micrometer, we measured a range for the membrane thicknesses rather than a single value (Table 3), since the membrane has some ability to shrink/contract based on the applied stress. The thickness of all the tested materials shrunk after drying except FKS whose minimum dry thickness was larger than its minimum wet thickness. As the membrane is more brittle when dry, its dry thickness lies within a narrower range compared to the wet range. We calculated the swelling percentage in the membrane length (S_{length}) and thickness ($S_{thickness}$) for each sample as follows

$$S_{length} = \frac{\sqrt{A_{wet}} - \sqrt{A_{dry}}}{\sqrt{A_{dry}}} \qquad \text{Eq. 31}$$

$$S_{thickness} = \frac{\delta_{m,wet} - \delta_{m,dry}}{\delta_{m,dry}} \qquad \text{Eq. 32}$$

where A is the area of the membrane sample. It was not practical to measure the dry area of the FKD samples as they coil up upon drying.

The average swelling percentage in the membrane thickness was calculated based on the average of the measured wet and dry thickness ranges (Fig. 4). Moreover, we estimated the maximum and minimum thickness swelling, e.g., the maximum swelling was calculated using the maximum wet thickness and the minimum dry thickness. While the membrane thickness was estimated by a range, the membrane length is measured as a single value. Approaching the membrane surface with a

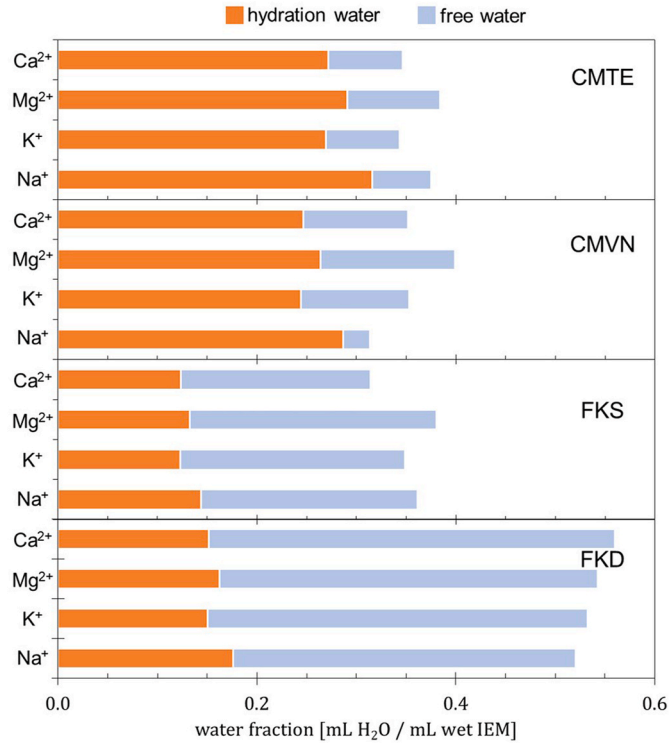

Fig. 8. Break-down of the membrane water volume fraction into hydration and free water.

desk micrometer can significantly influence the measured membrane thickness. However, this effect is insignificant for the membrane length measurement (by approaching the membrane edges with a caliper) owing to the higher scale of membrane length (mm) compared to its thickness (μm). The membrane swelling along its length (S_{length} range: 1 – 6 %) is more confined compared to its thickness ($S_{thickness,\ avg}$ range: 3 to 17 %). Generally, the thickness swelling is significantly higher than the length swelling. Since all the tested IEMs contain a reinforcement mesh which might swell differently compared to the membrane polymer, the membrane swelling along its length is limited relative to the thickness swelling.

In line with Taylor [36], the uncertainties are reported with one significant figure, and the average values are rounded accordingly (Table 4). The measured IEC values are in good agreement with the literature and with the tabulated values of the manufacturers. Furthermore, we calculated the ICD based on Eqs. 1a and 1b where CMTE, CMVN, and Fuji-T10 exhibited a relatively high ICD compared to the other three materials. Both concentration units, i.e., [mol/L water sorbed] or [mol/L swollen polymer]), can be used to describe the ion equilibria in membranes. Kamcev et al. [8] fitted the membrane equilibrium with an aqueous solution of NaCl. The authors plotted the activity coefficients inside the membrane in case of expressing the concentrations as either "moles/L sorbed water" or "moles/L swollen polymer" (Fig. 7a and Fig. S2 in Ref. [8], respectively). Both approaches led to similar trends of the membrane activity coefficients but the scale of the values is different in response to the scale of the used concentration units.

Following the basis of Eq. 1a, the aqueous solution is considered to be in equilibrium with the water inside the membrane. We assumed that the water density, applied in Eq. 1a, is same as the bulk water density. This assumption is not fully accurate since the IEMs have a high concentration of ions whose hydration shells contain water of lower molar volume (or density) relative to the bulk water, i.e., about 15 relative to 18 cm^3/mol [42,43], respectively. Nevertheless, the bulk water density was used in Eq. 1a; to be consistent with the calculations in literature, and to avoid the uncertainty about the exact hydration volume of the ions inside the membrane.

Following the basis of Eq. 1b, the membrane system is treated as two-phase equilibria: one is the aqueous solution while the other phase is the overall swollen membrane. However, Eq. 1b is not fully accurate since each membrane contains a different reinforcement material (also called backing material, Table 3) whose volume is inaccessible for ion transport. Therefore, we need to base our calculations on the effective or active swollen polymer volume as follows

$$ICD_e = \frac{ICD}{1 - f_b} \quad \text{Eq. 33}$$

where ICD_e is the effective ionic charge density. Galizia et al. [15] calculated the volume occupied by the backing in a commercial membrane, i.e., CR61. Their equation (Eq. S9 in Ref. [15]) can be rearranged to calculate the volume fraction of the backing (reinforcement) material in the swollen polymer (f_b)

$$f_b = \frac{V_b}{V_m} = \frac{\delta_b}{\delta_m}(1 - \varepsilon_b) \quad \text{Eq. 34}$$

where V_b and V_m are the volume of the backing and wet IEM, respectively. The calculations in our study were not corrected for the inactive reinforcement volume since each of the studied membranes has a different backing of an unknown thickness (δ_b) and porosity (ε_b).

We compared the calculated ICD to the values recently reported by Espinoza et al. [39] for CMVN, Fuji-T10, and Fuji-T12 (Table 4). There is a good agreement between the two studies for the ICD_b [mol/L swollen polymer], calculated via Eq. 1b. However, there are significant differences in the values of ICD_a [mol/L water sorbed], calculated via Eq. 1a. As discussed later, the water content measurement technique plays a major role, leading to such differences (Table SI- 8).

3.2. Water content measurement

In Fig. 5a, we compare the measured water content based on the different methods to remove the surface water film. For single membrane measurements (techniques: A – D as introduced in the Methods), we can calculate the standard deviation in the measurements, which reflects the measurement precision but not its accuracy. Therefore, we used the theory of Mackie and Meares [44] to calculate the theoretical membrane water content that corresponds to its measured EIS resistance (details of the theory and the calculations are given in the next sections,

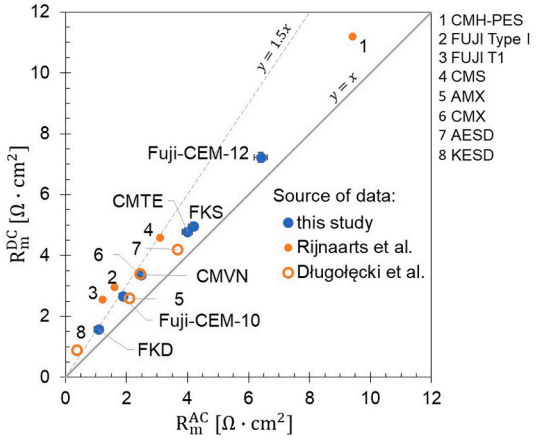

Fig. 9. Membrane resistance measurements based on direct current (DC, y-axis) compared to the alternating current (AC, x-axis). The blue circles are measured in the present study, where error bars in both x- and y-directions are added based on the uncertainty in each measurement (refer to the Methods sections for details). The smaller closed and open orange circles are measured by Rijnaarts et al. [76] and Długołęcki et al. [34], respectively.

and the Supporting Info, SI-1). This theoretical water content represents the minimum water content that the membrane should contain to provide the measured resistance in case the membrane tortuosity is the only factor contributing to the membrane resistance. Furthermore, the membrane water content might exceed this theoretical value while having the same conductivity since (a) the membrane might contain dead cavities that do not function as transport channels either because they are not connected or too narrow compared to the ion size, and (b) there are other sources of resistance inside the membrane such as the electrostatic interactions [21].

For single membrane measurements (A – D as introduced in the Methods), we found significant variations in the measured WC (Fig. 5a, Figure SI- 4). Generally, using a tissue/paper to directly remove the water film from the membrane surface underestimated the membrane water content (method B – D). The tissue can easily withdraw the water inside the membrane that is not associated with the hydration shell of the present ions. As we explain later, this is the case for FKS and FKD (Fig. 8). Using different tissue materials led to significant variations in the calculated WC, especially for CMVN. In case of membranes with low excess water (e.g., CMTE and CMVN), the membrane water content either favors staying in the ionic hydration shell or moving to the tissue depending on the absorption capacity of the tissue/paper and the ionic hydration energy.

Using the stacking method, we obtain 8 measurement points (Fig. 5b and c) for each membrane at equilibrium with a certain solution. The water content of the membrane was obtained from the slope of the linear fitting of these points (Eq. 4). Moreover, we calculated a confidence interval for the WC (membrane stacking method, Fig. 5a), which includes the WC value with a 90 % confidence level as described by Eq. 10–13. The more data points (N) to be used in the regression, the lower the standard error in b_1 as well as the t-factor, and consequently, we reach to a narrower confidence interval for the WC. The fitting parameters are summarized in the supplementary info (SI-3). A regression model that well explains the variability in the y measurements has a coefficient of determination (R^2) [26] close to 1. In this study, all fittings had high R^2 values (above 0.994) except for one measurement, FKS at 10 mM HCl ($R^2 = 0.985$). The measurement of CMTE and FKS at 0.5 M NaCl were reproduced twice, showing a good agreement since their WC values (stacking method) lie within the error margins or confidence intervals of the repeated measurements (Fig. 5a).

The effect of salinity on the water content of IEMs was compared to literature. Kamcev et al. [8,45] as well as Galizia et al. [15] observed a decreasing water content for three CEMs (CR61, CA267, and CA238) in response to increasing the solution salinity. Ji et al. [46] measured the water content of CMV, CMI-7000s, and XLAMPS at 0.1 and 0.5 M NaCl, where the difference between the two values was insignificant (within the error margins).

In our study (Fig. 6), we found that membranes of high ion-exchange capacity (i.e., CMTE and Fuji-T10) have a constant water content within the studied concentration range of 0.01 – 1 M NaCl. The other membranes had a fairly constant WC for ionic strengths <0.5 M NaCl. Moving towards higher ionic strength (0.5 – 1 M NaCl), the water content showed a slight increase (CMVN and Fuji-T12) or decrease (FKS). On one hand, the higher ionic strength of the solution lowers the osmotic pressure difference between the membrane and the solution, leading to osmotic de-swelling of the free water inside the membrane (water not bound to the ionic hydration shell). On the other hand, increasing solution salinity promotes co-ion leakage into the membrane which enhances the membrane swelling since those leaked ions enter the membrane with their (partial) hydration shell. Note that mobile salts inside the membrane at high solution salinity (1 M NaCl) are not included in the dry mass of the membrane since we soaked the membranes in demi water prior to drying. If the membranes were dried without soaking in demi water, the dry mass of the samples is expected to vary significantly in case of the measurements at concentrated solutions (>0.5 M NaCl). Again, those variations will depend on the way of removing the surface water film before drying.

3.3. Counter-ions influence on membrane swelling

We monitored the exchange of the membrane counter-ions (Table 5). Although CMTE is almost twice as thick as the other three membranes, FKS and FKD showed lower conversions using 0.2 M KCl and 0.1 M $MgCl_2$. Having high background concentrations of K^+ or Mg^{2+} can interfere with the measurement of the co-existing ions which is likely to influence the results of FKS and FKD more than the other membranes. Both FKS and FKD have low IEC (Table 4) and hence low amounts of counter-ions to be transferred to the exchange solution compared to the other membranes (for the same sample area). The ICP interference issue was avoided when using a low concentration of $CaCl_2$ solution. A concentration as low as 0.01 M $CaCl_2$ gave high conversions overall (>95 %) due to the high Ca^{2+} selectivity in CEMs according to the general selectivity sequence reported by Helfferich [5].

Fig. 7 illustrates the impact of the counter-ions on the membrane water content. Generally, the water content is higher when the membranes are in H^+ counter-ion form compared to the other forms. Similar results were observed in the study of Tuan et al. [7], where CMV membranes swelled further when soaked in acids (water content order: HCl > H_2SO_4 > NaCl). Several studies [47–50] introduced the concept of proton structure in aqueous solutions to explain the transport mechanism of protons and their unique mobility performance. Those authors pictured a hydronium ion that maintains three water molecules in its first hydration shell via hydrogen bonding, i.e., the Eigen configuration ($H_9O_4^+$). Another proposed configuration is the Zundel ion ($H_5O_2^+$), a proton shared between two water molecules. Further research is still needed to elucidate the proton interactions and its hydration shell structure inside IEMs, especially the proton selective and the proton resistive membranes.

Regarding the Na^+, K^+, Mg^{2+}, and Ca^{2+} ions, the counter-ion form influenced the membrane water content results, however, without a general trend (Fig. 7). Moreover, the changes in the membrane water content are not significant relative to the measurement uncertainty (confidence interval), especially for the FKD. Some trends for membrane water content for different counter-ions were reported in the literature [15,45] with similarity to the membrane selectivity trend. Nevertheless, no thermodynamic relation has been put forward to explain these two trends, as was also stated by Bonner et al. [51].

The membrane water content can be further analyzed in light of the ion solvation. Generally, the water content of an ion-exchange resin is considered either “hydration” or “free” water [5,52–55]. Although the meaning of the results can vary across the literature based on the adopted treatment, the experimental method, or the definition of the hydration shell. In our analysis, the hydration number ($\lambda^m_{hyd.}$ [mol H_2O/mol eq.]) refers to the number of water molecules (per equivalent mole of counter-ions) that are associated with the (primary and secondary) hydration shells of the mobile and fixed ions in the swollen membrane.

In studies of ion-exchange resins, the D’Arcy and Watt equation [56] was frequently used to calculate the hydration number of the resin by fitting the water vapor sorption isotherm data [53,57–59]. This approach employs different parameters that associate the water to strong or weak hydration sites, or multilayer formation (free water). However, Nandan et al. [53] showed this analysis only distinguished the primary hydration for some counter-ion species such as Na^+.

For the sake of a consistent comparison, we assumed all counter-ions to be fully hydrated inside the membrane with radii similar to their recorded radii in solution. This translates to estimating the maximum limit for the hydrated water and the minimum limit for the free water. Burgess [60,61] provided a comprehensive review of the different methods for estimating the hydration numbers of ions. The radii, used in our analysis, are based on the electrolyte transport properties [62,63]

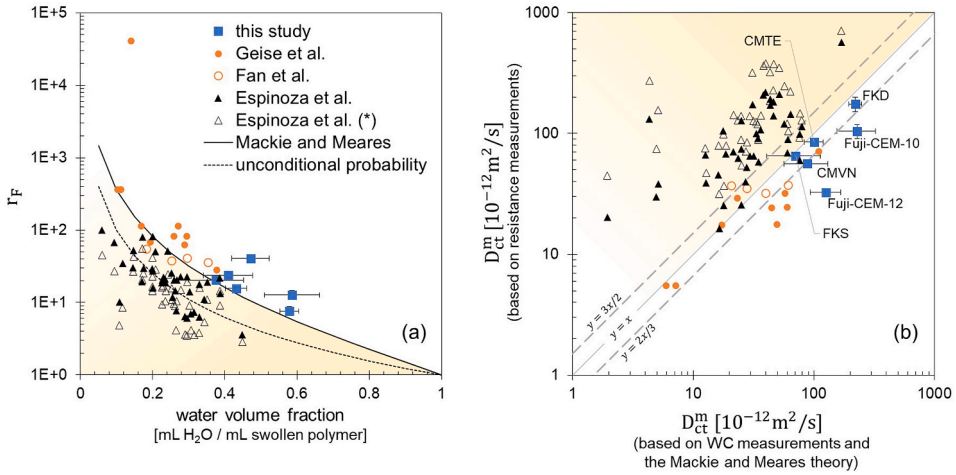

Fig. 10. (a) The reduction factor (r_F, y-axis) for the counter-ion mobility inside ion-exchange membranes compared to the water volume fraction of the membrane (x-axis). The markers present the reduction factors calculated based on the resistance measurements. The theoretical reduction factor of the ion mobility for an arbitrary membrane water volume fraction is plotted based on Mackie and Meares (solid line) or the unconditional probability (dashed line, details are provided in the Supporting Info, SI-1). (b) The diffusion coefficient of counter-ions inside the membrane based on resistance measurements (y-axis) versus the value calculated via the Mackie and Meares equation (x-axis). A thin solid line represents the function: y = x, while the two dashed lines represent a multiplication or division factor of 1.5. In both figures, the blue squares represent CEMs based on this study (r_F is based on EIS measurements, and WC was measured via the stacking method). The data marked by the solid and hollow orange circles come from the study of Geise et al. [18] and Fan et al. [21], respectively (r_F is based on DC resistance measurements, and WC was measured via method B). For the data points of Espinoza et al. [39], the WC was measured via method B, and the r_F is calculated based on the EIS resistance measurements (solid triangles) or based on the reported membrane diffusion coefficients in the originating study (hollow triangles). All data points are provided in Table SI- 7.

(Table 6). CEMs commonly have sulfonate groups ($R–SO_3^-$) as their fixed-charged groups [2,64–66]. Due to a lack of data, we assumed the radii of the fixed-charged groups to be similar to chloride ions rather than the (divalent) sulfates.

We adapted Eq. 3, in Ref. [43], to estimate the volume of water associated with the hydration shell of an equivalent mole of ions (i) ($V^{eq.}_{hyd.,i}$ [mL H_2O/mol eq.]) as follows

$$V^{eq.}_{hyd.,i} = \frac{4\pi \cdot A_v}{3 \cdot |z_i|}\left(r^3_{H,i} - r^3_{C,i}\right) \quad \text{Eq. 35}$$

where A_v is Avogadro's number (6.02E+23 ion/mol). The hydrated and crystal radii of ion (i) are given by $r_{H,i}$ and $r_{C,i}$ [A°], respectively. At 10 mM of chloride salts, ions inside the membranes are basically counter-ions and fixed-charged groups. In this case, the co-ion concentration can be neglected. The hydration number is calculated as follows

$$\lambda^m_{hyd.} = \frac{\sum_i V^{eq.}_{hyd.,i}}{\overline{V^{HS}_{H_2O}}} \quad \text{Eq. 36}$$

where "i" refers to all the ionic species inside the membrane. The molar volume of water inside the hydration shell ($\overline{V^{HS}_{H_2O}}$) was estimated to be 15 mL H_2O/mol H_2O [42,43]. The volume fraction of water associated with the ionic hydration shells inside the membrane ($V_{hyd.}$ [mL H_2O/mL wet IEM]) is given by

$$V_{hyd.} = ICD \cdot \sum_i V^{eq.}_{hyd.,i} \quad \text{Eq. 37}$$

Furthermore, the free water fraction ($V_{free\ water}$) represents the difference between the measured water content and the hydration number as follows

$$V_{free\ water} = \frac{\left(WC - \lambda_{hyd.} \cdot IEC \cdot M_{H_2O}\right) \cdot \rho_m}{\rho_{free\ water}} \quad \text{Eq. 38}$$

where M_{H_2O} [g/mol] is the molar mass of water. The free water density, $\rho_{free\ water}$, was assumed to be the same as the bulk water density, i.e., 0.998 g H_2O/mL H_2O at 20 °C [67].

Generally, the counter-ion species inside the membrane have a minor influence on the hydration water inside the membrane (Fig. 8). For some membranes, e.g., FKD, those differences in the hydration water volume (Fig. 8) are within the uncertainty of the WC measurement (Fig. 7). Unbound to any hydration shell, the free water inside the membrane is the fraction that is mostly influenced by the osmotic effect of the solution. Converting from Na^+ to K^+ form (or Mg^{2+} to Ca^{2+}), we obtain the same number of counter-ions with similar hydration energy, but with smaller hydration numbers (Table 6). Therefore, the membrane water content is expected to be relatively lower, i.e., $WC_K < WC_{Na}$ (also $WC_{Ca} < WC_{Mg}$). This is the case for the CMTE and FKS membranes (Fig. 8).

The hydration energy of divalent ions is significantly higher than that of monovalent ones (Table 6). Although the degree of dehydration of ions inside the membrane is unknown, monovalent ions are expected to get further dehydrated compared to the divalent ions. The degree of dehydration does not only depend on the ion properties, but also on the swollen membrane structure. In Fig. 8, we illustrate the breakdown of the membrane water volume fraction at equilibrium with 10 mM of different chloride solutions, e.g., 10 mM of $CaCl_2$. For each membrane material, the osmotic pressure difference between the membrane and the solution is almost the same for the different counter-ions. Therefore, the free water portion inside the membrane is expected to be similar in all forms. However, the free water in the Na^+ form of CMVN is significantly smaller relative to other forms of the same membrane. Therefore, the sodium ions are likely to face more pronounced dehydration in CMVN relative to the other cations in this membrane. The dehydration extent of counter-ion depends on the hydration energy as well as the effective diameter of the membrane cavities or transport channels [70–72].

3.4. Water content influence on the ion mobility

Picturing (partially) hydrated ions and the different water fractions inside the membrane (Fig. 8), we expect some influences for the free and overall water volume fractions on the transport, and consequently the membrane performance. Firstly, a membrane with a high free water

fraction is likely to have a high water permeability and hence a high osmotic water leakage. In this regard, the osmotic water leakage is expected to be higher for FKD relative to the other membranes (FKD > FKS > CMVN, CMTE). This can be supported by the study of Dražević et al. [73] who showed an increasing trend for the water intrinsic permeability in aromatic polyamide (reverse osmosis, RO) membranes as their water content is raised. While both IEMs and RO membranes contain a dense polymeric layer, RO membranes do not contain a significant number of fixed charges compared to IEMs. Therefore, we can consider the whole RO membrane water content as free water, i.e., unlimited by the ionic hydration energy.

Secondly, higher ionic mobilities are expected in the membrane with higher free water content. More free water inside the membrane translates to more space for ions to move with low friction between the ions and the membrane polymer as well as among themselves (solute-membrane and solute-solute friction). Kingsbury et al. [6] studied the water permeation for 20 commercial IEMs and concluded that the water and salt permeability are highly correlated to one another regardless of polymer type or reinforcement. Such a correlation does not imply causality. Instead, it is a common membrane parameter that influences both water and salt permeabilities in the same way, either positively or negatively.

To cross a membrane, the ions need to take a longer diffusion path relative to their path if they were to cross a pure solution of the same thickness, i.e., membrane tortuosity [74,75]. Therefore, the mobility inside the membrane is reduced by a factor (r_F)

$$r_F = \frac{u_i}{u_i^m} = \frac{D_i}{D_i^m} \quad \text{Eq. 39}$$

where u_i and D_i are the mobility and diffusion coefficient of ion (i) in aqueous solutions. Subscript, m, refers to the swollen membrane phase. The diffusion coefficient for Na^+ and Cl^- in aqueous solutions equals 1.33E-9 and 2.03E-9 m^2/s respectively [67].

Mackie and Meares [44] postulated a theoretical framework to account for the effect of tortuosity using only one parameter: the water fraction in the membrane. They described the swollen membrane phase using a cubic lattice (Figure SI- 1b), where an ion at position (0) has a coordination number of 6. Each position around the ion can be either occupied by the membrane polymer, a hydrated ion, or water molecules. As the polymer chain mobility is much lower than that of ions, the sites occupied by the polymer are unavailable for the ions. Their analysis concludes with a simple relation between the water volume fraction and the mobility reduction factor of the membrane (details in the Supporting Info, SI-1)

$$r_F^{Mackie} = \left(\frac{2 - V_w}{V_w}\right)^2 \quad \text{Eq. 40}$$

To evaluate the accuracy of Mackie and Meares's theory in explaining the experimental observations, we also calculated the ion diffusion coefficient inside the membrane based on the resistance measurement. We measured the membrane resistance via two approaches: electrochemical impedance spectroscopy (EIS) as well as direct current (DC) at 0.5 M NaCl (Fig. 9, Figure SI- 5). We included results from Rijnaarts et al. [76] and Długołęcki et al. [34] as they also measured the membrane resistance via both approaches. Długołęcki et al. [34] measured the membrane resistance at three different flow rates. We selected their measurements at the highest flow rate (0.8 l/min); because they did their measurements using a 2-compartment cell where one solution is flowed between the membrane and the working or counter electrodes. In other words, using a higher flow rate is better to reduce the influence of the electrode reactions on the ionic composition of the solution and membrane under investigation. Although the resistance of Ralex CMH-PES is relatively high compared to the other membranes (point no. 1 in Fig. 9), this traces back to its relatively high thickness (680 μm [76]) rather than having a heterogenous structure since it exhibited a relatively low-to-moderate specific resistivity (Figure SI- 6).

The membrane resistance, measured by EIS, was always lower than that based on DC measurement (Fig. 9) for two reasons: (a) Using EIS, we can differentiate between the membrane resistance and the interfacial resistances such as the diffusion boundary layer resistance [34,77] that develops at the membrane surface. On the other hand, the DC method measures the combined resistance of the membrane and interfacial resistances. (b) During EIS measurement, an alternating current was applied at open circuit voltage where the ions oscillate in response to the frequency of the applied signal. Friction between ions and the membrane polymer is less significant when the ions are oscillating (EIS measurement) compared to actually crossing the membrane (DC measurement). For common applications of IEMs, such as electrodialysis, the DC method provides further insights into the overall ion-transport resistance. In this study, we compared the theory of Mackie and Meares to the measured EIS resistance instead of the DC resistance since the former better represents the membrane tortuosity.

We considered a membrane in equilibrium with a 0.5 M NaCl solution. Neglecting the activity coefficients in the solution and membrane, the Donnan equilibrium condition [35,78] simplifies to

$$\left(\frac{C_{Na^+}^m}{C_{Na^+}}\right)^{1/z_{Na^+}} = \left(\frac{C_{Cl^-}^m}{C_{Cl^-}}\right)^{1/z_{Cl^-}} \quad \text{Eq. 41}$$

Furthermore, the concentrations of mobile ions inside the membrane (C_i^m [mol / L swollen polymer]) are governed by the electroneutrality condition:

$$z_{fix} \cdot C_{fix}^m + \sum_i z_i \cdot C_i^m = 0 \quad \text{Eq. 42}$$

where C_{fix}^m equals the ICD_b and z_{fix} is the charge of the fixed ions (equals −1). We solved Eqs. 41 and 42 for the concentration of the counter- (Na^+) and co- (Cl^-) ions inside the membrane.

Einstein-Smoluchowski equation [79] relates the diffusion coefficient of an ion (D_i) to its mobility (u_i) via

$$u_i^m = \frac{|z_i| \cdot F \cdot D_i^m}{R \cdot T} \quad \text{Eq. 43}$$

where F [C/mol], R [J/(K·mol)], and T [K] are Faraday's constant, the universal gas constant, and the temperature (293 K), respectively. For each membrane material (j), one mobility reduction factor ($r_{F,j}$) was assigned for Na^+ and Cl^-. Moreover, we assumed a homogenous membrane where counter- and co-ions are uniformly distributed and contribute to the membrane conductivity. Hence, the membrane conductivity (κ_m) [35,79] is proportional to the ionic charge, mobility, and concentration via

$$\kappa_m = F \sum_i |z_i| \cdot u_i^m \cdot C_i^m \quad \text{Eq. 44}$$

By solving Eqs. 39, 43, and 44, we calculated the diffusion coefficient of Na^+ inside each membrane material.

In our analysis, we included the relevant data from literature: Geise et al. [18] measured the membrane-area resistance and the water volume fraction for 10 types of AEMs at 0.5 M NaCl. Fan et al. [21] reported the membrane conductivity and the water volume fraction for 4 commercial IEMs at 1 M NaCl. Furthermore, Espinoza et al. [39] characterized 40 different commercial membranes at 1 M NaCl. They calculated the counter- and co-ion diffusion coefficients inside the membrane based on measuring the membrane resistance (EIS, direct-contact method), the ion concentrations in the membrane (the membrane was wiped to remove the surface water film, method B), and the salt permeability. We analyzed the data from Espinoza et al. in two ways: firstly, we used the reported membrane conductivity data and applied the aforementioned approach (Eq. 41–44) to solve for the ion diffusion coefficient inside the membrane (solid triangles, Fig. 10).

Secondly, we directly used the reported diffusion coefficients by the authors (hollow triangles, Fig. 10).

Generally, the membrane water volume fraction positively influences the ion mobility inside the membrane (Fig. 10a) as it leads to a lower tortuosity reduction factor. This trend (Fig. 10a) is more consistent compared to the trend of the membrane-specific resistance against the membrane water volume fraction (Fig. 5 in Ref. [18]). The ion mobility inside IEMs (or its reduction factor) depends on the nature of the ion as well as the membrane structure, e.g., the tortuosity and the size of the transport channels of the membrane. However, the intrinsic membrane resistance depends on the concentration of mobile ions and their mobilities inside the membrane as given in Eq. 44.

In Fig. 10b, we compare the diffusion coefficient inside the membrane based on two approaches: (a) Mackie and Meares theory (Eq. 40) versus (b) the resistance measurement (Eq. 44). The reduction in ion mobility is well explained by the tortuosity for 4 out of the 6 membranes characterized in our study. The Fujifilm membranes, i.e., T10 and T12, exhibited an ion diffusion coefficient (based on the measured resistance) that is more than 1.5x lower than the prediction based on Mackie and Meares theory. This can be explained by: (a) the tortuosity of the membrane structure can be more intricate than the treatment of Mackie and Meares since the membrane might contain dead cavities that contribute to the water content but not to the membrane conductivity, (b) there are measurement errors in the WC, and (c) the membrane tortuosity is one among other factors that contribute to the membrane resistance, and consequently, to the reduction factor of the ion mobility [21]. For the data of Geise et al. [18] and Fan et al. [21], the membrane resistance is measured via the DC method which includes frictional factors in the resistance beside the membrane tortuosity.

Generally, the membrane must contain a minimum amount of water to justify a specific conductivity. The ion diffusion coefficient, based on the membrane resistance, is expected to be lower than the predicted value by the Mackie and Meares theory which accounts for the tortuosity resistance only. However, most of the data points, retrieved from Ref. [39], showed significantly (exceeding 1.5 times) higher diffusion coefficients (based on the measured resistance) compared to the calculated values based on the membrane water volume fraction and the Mackie and Meares theory (grey triangles in Fig. 10b). We hypothesize that this departure from the theory mainly originates from the experimental technique of the WC measurement. We compared the results for three commercial membranes characterized in our study with the values given in Ref. [39] (Table SI- 8). Between the two studies, the relative differences in values for the IEC, the membrane thickness, and the membrane-area resistance range from −11 to +28 %. However, the membrane WC values measured in our study (stacking method) are higher by 110 – 145 % relative to the values in Ref. [39] (method B). Therefore, the WC measurement technique led to major differences in the results as explained earlier in Fig. 5a. The WC values in Ref. [39] are hypothesized to be underestimated because (a) they are mostly below the minimum WC values that explain the measured conductivities (Fig. 10), and (b) they lead to the ionic charge densities of 1 – 15 mol/L sorbed water (Fig. 1b in Ref. [39]). Such concentrations of counter-ions are quite high relative to the solubility limits of the common sodium salts (Table SI- 9, e.g. solubility of NaCl is 6.1 mol/L water at 25 °C).

The error bars in the x- and y-directions (Fig. 10) reflect the uncertainty in the membrane water volume fraction and conductivity, respectively. The error in the water volume fraction propagates from the WC, the membrane surface area density, and the wet membrane thickness measurements. The error in the membrane diffusion coefficient propagates from the membrane resistance and wet membrane thickness measurements. Generally, the uncertainty in the diffusion coefficient based on the membrane conductivity is small compared to the one based on the water volume fraction.

4. Conclusion

We investigated the water content (WC) of six commercial CEMs via a new measurement technique (membrane stacking). This technique minimized the impact of the surface water film on the membrane without the need of wiping the membrane surface. Moreover, the data fitting approach provides a confidence interval of the water content value to judge the accuracy of the technique. We analyzed the membrane WC either as free water or hydration water, assuming that the ions are fully hydrated inside the membrane. Generally, the change in the hydration water due to changing the counter-ion species (from Na^+ to K^+, Mg^{2+}, or Ca^{2+}) is not significant relative to the WC measurement uncertainty.

To explore the influence of the WC on the ion mobility inside the membrane, we measured the membrane resistance via two methods: electrochemical impedance spectroscopy (EIS) and direct current (DC). The EIS-measured resistance was always lower than the corresponding DC measurement since the ions are oscillating (EIS) rather than moving (DC). Based on the stacking WC measurements and the EIS resistance measurements, there is a positive trend between the membrane water volume fraction and its ion mobility which is explained by the membrane tortuosity.

CRediT authorship contribution statement

Alaaeldin A.E. Elozeiri: Writing – review & editing, Writing – original draft, Visualization, Methodology, Investigation, Formal analysis, Data curation, Conceptualization. **Rob G.H. Lammertink:** Writing – review & editing, Visualization, Supervision, Methodology, Funding acquisition, Formal analysis, Conceptualization. **Huub H.M. Rijnaarts:** Writing – review & editing, Visualization, Supervision, Methodology, Funding acquisition, Formal analysis, Conceptualization. **Jouke E. Dykstra:** Writing – review & editing, Visualization, Supervision, Methodology, Funding acquisition, Formal analysis, Conceptualization.

Declaration of competing interest

The authors declare that they have no known competing financial interests or personal relationships that could have appeared to influence the work reported in this paper.

Data availability

Data will be made available on request.

Acknowledgements

This research was performed within the framework of the research program AquaConnect, funded by the Dutch Research Council (NWO, grant-ID P19-45) and public and private partners of the AquaConnect consortium and coordinated by Wageningen University and Research.

Appendix A. Supplementary data

Supplementary data to this article can be found online at https://doi.org/10.1016/j.memsci.2024.122538.

References

[1] T. Xu, Ion exchange membranes: State of their development and perspective, J. Membr. Sci. 263 (1–2) (Oct. 2005) 1–29, https://doi.org/10.1016/j.memsci.2005.05.002.
[2] J. Ran, et al., Ion exchange membranes: new developments and applications, J. Membr. Sci. 522 (Jan. 2017) 267–291.
[3] T. Luo, S. Abdu, M. Wessling, Selectivity of ion exchange membranes: a review, J. Membr. Sci. 555 (December 2017) (Jun. 2018) 429–454, https://doi.org/10.1016/j.memsci.2018.03.051.

[4] T. Sata, T. Sata, W. Yang, Studies on cation-exchange membranes having permselectivity between cations in electrodialysis, J. Membr. Sci. 206 (1–2) (Aug. 2002) 31–60, https://doi.org/10.1016/S0376-7388(01)00491-4.

[5] F.G. Helfferich, Ion Exchange, no. 3, McGraw-Hill, 1962.

[6] R.S. Kingsbury, S. Zhu, S. Flotron, O. Coronell, Microstructure determines water and salt permeation in commercial ion-exchange membranes, ACS Appl. Mater. Interfaces 10 (46) (Nov. 2018) 39745–39756, https://doi.org/10.1021/acsami.8b14494.

[7] L.X. Tuan, M. Verbanck, C. Buess-Herman, H.D. Hurwitz, Properties of CMV cation exchange membranes in sulfuric acid media, J. Membr. Sci. 284 (1–2) (Nov. 2006) 67–78, https://doi.org/10.1016/j.memsci.2006.06.036.

[8] J. Kamcev, D.R. Paul, B.D. Freeman, Ion activity coefficients in ion exchange polymers: Applicability of Manning's counterion condensation theory, Macromolecules 48 (21) (Nov. 2015) 8011–8024, https://doi.org/10.1021/acs.macromol.5b01654.

[9] P. Długołecki, K. Nymeijer, S. Metz, M. Wessling, Current status of ion exchange membranes for power generation from salinity gradients, J. Membr. Sci. 319 (1–2) (Jul. 2008) 214–222, https://doi.org/10.1016/j.memsci.2008.03.037.

[10] H.K. Kim, M.S. Lee, S.Y. Lee, Y.W. Choi, N.J. Jeong, C.S. Kim, High power density of reverse electrodialysis with pore-filling ion exchange membranes and a high-open-area spacer, J. Mater. Chem. A 3 (31) (Jul. 2015) 16302–16306, https://doi.org/10.1039/C5TA03571F.

[11] L. V Karpenko-Jereb, N.P. Berezina, Determination of structural, selective, electrokinetic and percolation characteristics of ion-exchange membranes from conductive data, Desalination 245 (1–3) (Sep. 2009) 587–596, https://doi.org/10.1016/j.desal.2009.02.024.

[12] T. Luo, Y. Zhong, D. Xu, X. Wang, M. Wessling, Combining Manning's theory and the ionic conductivity experimental approach to characterize selectivity of cation exchange membranes, J. Membr. Sci. 629 (Jul. 2021) 119263, https://doi.org/10.1016/j.memsci.2021.119263.

[13] G.Q. Chen, K. Wei, A. Hassanvand, B.D. Freeman, S.E. Kentish, Single and binary ion sorption equilibria of monovalent and divalent ions in commercial ion exchange membranes, Water Res. 175 (May 2020) 115681, https://doi.org/10.1016/j.watres.2020.115681.

[14] C. Hannachi, M.B.S. Ali, B. Hamrouni, Determination of the selectivity coefficient of the CMX cationic membrane at various ionic strengths, Desalin. Water Treat. 10 (1–3) (Oct. 2009) 47–52, https://doi.org/10.5004/dwt.2009.725.

[15] M. Galizia, F.M. Benedetti, D.R. Paul, B.D. Freeman, Monovalent and divalent ion sorption in a cation exchange membrane based on cross-linked poly (p-styrene sulfonate-co-divinylbenzene), J. Membr. Sci. 535 (Aug. 2017) 132–142, https://doi.org/10.1016/j.memsci.2017.04.007.

[16] E. Güler, R. Elizen, D.A. Vermaas, M. Saakes, K. Nijmeijer, Performance-determining membrane properties in reverse electrodialysis, J. Membr. Sci. 446 (Nov. 2013) 266–276, https://doi.org/10.1016/j.memsci.2013.06.045.

[17] Sarapulova, et al., Transport characteristics of fujifilm ion-exchange membranes as compared to homogeneous membranes AMX and CMX and to heterogeneous membranes MK-40 and MA-41, Membranes 9 (7) (Jul. 2019) 84, https://doi.org/10.3390/membranes9070084.

[18] G.M. Geise, M.A. Hickner, B.E. Logan, Ionic resistance and permselectivity tradeoffs in anion exchange membranes, ACS Appl. Mater. Interfaces 5 (20) (Oct. 2013) 10294–10301, https://doi.org/10.1021/am403207w.

[19] M. Bass, V. Freger, Hydration of Nafion and Dowex in liquid and vapor environment: schroeder's paradox and microstructure, Polymer (Guildf). 49 (2) (Jan. 2008) 497–506, https://doi.org/10.1016/j.polymer.2007.11.054.

[20] X.T. Le, et al., Diazonium-induced anchoring process: an application to improve the monovalent selectivity of cation exchange membranes, J. Mater. Chem. 20 (18) (Apr. 2010) 3750, https://doi.org/10.1039/b918915g.

[21] H. Fan, Y. Huang, I.H. Billinge, S.M. Bannon, G.M. Geise, N.Y. Yip, Counterion mobility in ion-exchange membranes: spatial effect and valency-dependent electrostatic interaction, ACS ES&T Eng. 2 (7) (Jul. 2022) 1274–1286, https://doi.org/10.1021/acsestengg.1c00457.

[22] H. Miyoshi, M. Chubachi, M. Yamagami, T. Kataoka, Characteristic coefficients for equilibrium between solution and Neosepta or Selemion cation exchange membranes, J. Chem. Eng. Data 37 (1) (Jan. 1992) 120–124, https://doi.org/10.1021/je00005a031.

[23] J.-S. Park, T.C. Chilcott, H.G.L. Coster, S.-H. Moon, Characterization of BSA-fouling of ion-exchange membrane systems using a subtraction technique for lumped data, J. Membr. Sci. 246 (2) (Jan. 2005) 137–144, https://doi.org/10.1016/j.memsci.2004.07.022.

[24] S. Ozkul, et al., Transport mechanisms in electrodialysis: the effect on selective ion transport in multi-ionic solutions, J. Membr. Sci. 665 (Jan. 2023) 121114, https://doi.org/10.1016/j.memsci.2022.121114.

[25] D. Pintossi, C.-L. Chen, M. Saakes, K. Nijmeijer, Z. Borneman, Influence of sulfate on anion exchange membranes in reverse electrodialysis, npj Clean Water (Dec. 15, 2020). https://www-nature-com.ezproxy.library.wur.nl/articles/s41545-020-0073-7. (Accessed 9 October 2022).

[26] S.C. Chapra, R.P. Canale, Numerical Methods for Engineers, sixth ed., McGraw-Hill, New York, 2010.

[27] M. Bland, An Introduction to Medical Statistics, fourth ed., Oxford University Press, 2015.

[28] V. Bewick, L. Cheek, J. Ball, Statistics review 7: correlation and regression, Crit. Care 7 (6) (Dec. 2003) 451–459, https://doi.org/10.1186/cc2401.

[29] R.K. Nagarale, G.S. Gohil, V.K. Shahi, Recent developments on ion-exchange membranes and electro-membrane processes, Adv. Colloid Interface Sci. 119 (2–3) (Feb. 2006) 97–130, https://doi.org/10.1016/j.cis.2005.09.005.

[30] V. Sarapulova, et al., Supplementary Materials: transport characteristics of fujifilm ion-exchange membranes as compared to homogeneous membranes AMX and CMX and to heterogeneous membranes MK-40 and MA-41, Membranes 9 (7) (2019) 1–3, https://doi.org/10.3390/membranes9070084.

[31] S. Shi, A.Z. Weber, A. Kusoglu, Structure-transport relationship of perfluorosulfonic-acid membranes in different cationic forms, Electrochim. Acta 220 (Dec. 2016) 517–528, https://doi.org/10.1016/j.electacta.2016.10.096.

[32] A.H. Galama, et al., Membrane resistance: the effect of salinity gradients over a cation exchange membrane, J. Membr. Sci. 467 (Oct. 2014) 279–291, https://doi.org/10.1016/j.memsci.2014.05.046.

[33] T. Rijnaarts, D.M. Reurink, F. Radmanesh, W.M. de Vos, K. Nijmeijer, Layer-by-layer coatings on ion exchange membranes: effect of multilayer charge and hydration on monovalent ion selectivities, J. Membr. Sci. 570–571 (October 2018) (Jan. 2019) 513–521, https://doi.org/10.1016/j.memsci.2018.10.074.

[34] P. Długołęcki, P. Ogonowski, S.J. Metz, M. Saakes, K. Nijmeijer, M. Wessling, On the resistances of membrane, diffusion boundary layer and double layer in ion exchange membrane transport, J. Membr. Sci. 349 (1–2) (Mar. 2010) 369–379, https://doi.org/10.1016/j.memsci.2009.11.069.

[35] H. Strathmann, Ion-Exchange Membrane Separation Processes, first ed., Elsevier Science, Amsterdam, 2004.

[36] J.R. Taylor, An Introduction to Error Analysis: the Study of Uncertainties in Physical Measurements, second ed., University Science Books, 1997.

[37] "Ion Exchange Membranes: High-performance fumasep® ion exchange membranes for Electro Membrane Processes." [Online]. Available: http://www.fumatech.com/..

[38] Fujifilm - Ion Exchange Membranes for Water Purification, 2022 [Online]. Available: http://www.fujifilmmembranes.com/.

[39] C. Espinoza, D. Kitto, J. Kamcev, Counter-ion conductivity and selectivity trade-off for commercial ion-exchange membranes at high salinities, ACS Appl. Polym. Mater. (Nov. 2023), https://doi.org/10.1021/acsapm.3c02102.

[40] R. Wang, et al., Recovery of L-glutamic acid from ammonium glutamate by Donnan dialysis: membrane characteristic and operation parameters, J. Membr. Sci. 658 (Sep. 2022) 120766, https://doi.org/10.1016/j.memsci.2022.120766.

[41] W. Wang, R. Fu, Z. Liu, H. Wang, Low-resistance Anti-fouling Ion Exchange Membranes Fouled by Organic Foulants in Electrodialysis, 2017, https://doi.org/10.1016/j.desal.2017.05.013.

[42] D.R. Stranks, The elucidation of inorganic reaction mechanisms by high pressure studies, Pure Appl. Chem. 38 (3) (Jan. 1974) 303–323, https://doi.org/10.1351/pac197438030303.

[43] K. Shimizu, The contraction of water in the hydration shell, Bull. Chem. Soc. Jpn. 52 (8) (Aug. 1979) 2429–2430, https://doi.org/10.1246/bcsj.52.2429.

[44] J.S. Mackie, P. Meares, The diffusion of electrolytes in a cation-exchange resin membrane I. Theoretical, Proc. R. Soc. London. Ser. A. Math. Phys. Sci. 232 (1191) (Nov. 1955) 498–509, https://doi.org/10.1098/rspa.1955.0234.

[45] J. Kamcev, D.R. Paul, B.D. Freeman, Equilibrium ion partitioning between aqueous salt solutions and inhomogeneous ion exchange membranes, Desalination 446 (Nov. 2018) 31–41, https://doi.org/10.1016/j.desal.2018.08.018.

[46] Y. Ji, H. Luo, G.M. Geise, Specific co-ion sorption and diffusion properties influence membrane permselectivity, J. Membr. Sci. 563 (Oct. 2018) 492–504, https://doi.org/10.1016/j.memsci.2018.06.010.

[47] Y. Zeng, A. Li, T. Yan, Hydrogen bond dynamics in the solvation shell on proton transfer in aqueous solution, J. Phys. Chem. B 124 (9) (Feb. 2020) acs.jpcb.0c00990, https://doi.org/10.1021/acs.jpcb.0c00990.

[48] C.T. Wolke, et al., Spectroscopic snapshots of the proton-transfer mechanism in water, Science 354 (6316) (Dec. 2016) 1131–1135, https://doi.org/10.1126/science.aaf8425.

[49] D. Marx, M.E. Tuckerman, J. Hutter, M. Parrinello, The nature of the hydrated excess proton in water, Nature 397 (6720) (Feb. 1999) 601–604, https://doi.org/10.1038/17579.

[50] B. Kirchner, Eigen or Zundel ion: news from calculated and experimental photoelectron spectroscopy, ChemPhysChem 8 (1) (Jan. 2007) 41–43, https://doi.org/10.1002/cphc.200600476.

[51] O.D. Bonner, L. Lou Smith, A selectivity scale for some divalent cations on Dowex 50, J. Phys. Chem. 61 (3) (Mar. 1957) 326–329, https://doi.org/10.1021/j150549a011.

[52] E. Glueckauf, G.P. Kitt, A theoretical treatment of cation exchangers - III. The hydration of cations in polystyrene sulphonates, Proc. R. Soc. London. Ser. A. Math. Phys. Sci. 228 (1174) (Mar. 1955) 322–341, https://doi.org/10.1098/rspa.1955.0051.

[53] D. Nandan, B. Venkataramani, A.R. Gupta, Ionic hydration and water sorption isotherms of ion exchange resins, Langmuir 9 (7) (Jul. 1993) 1786–1793, https://doi.org/10.1021/la00031a029.

[54] H.D. Sharma, N. Subramanian, Proton magnetic resonance studies of ionic solvation in ion-exchange resins. Part II, Can. J. Chem. 49 (3) (Feb. 1971) 457–467, https://doi.org/10.1139/v71-071.

[55] K.W. Pepper, D. Reichenberg, D.K. Hale, "599. Properties of ion-exchange resins in relation to their structure. Part IV. Swelling and shrinkage of sulphonated polystyrenes of different cross-linking,", J. Chem. Soc. (1952) 3129, https://doi.org/10.1039/jr9520003129.

[56] R.L. D'Arcy, I.C. Watt, Analysis of sorption isotherms of non-homogeneous sorbents, Trans. Faraday Soc. 66 (0) (Jan. 1970) 1236, https://doi.org/10.1039/tf9706601236.

[57] R.S.D. Toteja, B.L. Jangida, M. Sundaresan, B. Venkataramani, Water sorption isotherms and cation hydration in Dowex 50W and amberlyst-15 ion exchange resins, Langmuir 13 (11) (May 1997) 2980–2982, https://doi.org/10.1021/la9607114.

[58] B. Venkataramani, Studies on the state of water present in ion exchangers, J. Ion Exch. 14 (Supplement) (2003) 101–104, https://doi.org/10.5182/jaie.14.Supplement_101.
[59] A.R. Gupta, An interpretation of water sorption isotherms of ion exchange resins, Indian J. Chem. 24A (1985) 368–372. Nov. 24, 2023. [Online]. Available: https://nopr.niscpr.res.in/bitstream/123456789/48630/1/IJCA, 24A(5) 368-372.pdf.
[60] J. Burgess, Metal Ions in Solution, Ellis Horwood, 1978.
[61] J. Burgess, Ions in Solution : Basic Principles of Chemical Interactions, second ed., Horwood Publishing, 1999.
[62] E.R. Nightingale, Phenomenological theory of ion solvation. Effective radii of hydrated ions, J. Phys. Chem. 63 (9) (Sep. 1959) 1381–1387, https://doi.org/10.1021/j150579a011.
[63] R.A. Robinson, R.H. Stokes, Electrolyte Solutions, second ed., R. Butterworths, 1965.
[64] T. Xu, D. Wu, L. Wu, Poly(2,6-dimethyl-1,4-phenylene oxide) (PPO)—a versatile starting polymer for proton conductive membranes (PCMs), Prog. Polym. Sci. 33 (9) (Sep. 2008) 894–915, https://doi.org/10.1016/J.PROGPOLYMSCI.2008.07.002.
[65] Y. Fujimura, T. Kawakatsu, M. Morimoto, H. Asakawa, K. Nakagawa, T. Yoshioka, Study for removing of silica nanoparticle in pure isopropyl alcohol with a cation exchange membrane, J. Mol. Liq. 367 (Dec. 2022) 120441, https://doi.org/10.1016/j.molliq.2022.120441.
[66] N.P. Berezina, N.A. Kononenko, O.A. Dyomina, N.P. Gnusin, Characterization of ion-exchange membrane materials: properties vs structure, Adv. Colloid Interface Sci. 139 (1–2) (Jun. 2008) 3–28, https://doi.org/10.1016/j.cis.2008.01.002.
[67] W.M. Haynes, D.R. Lide, T.J. Bruno (Eds.), CRC Handbook of Chemistry and Physics : a Ready-Reference Book of Chemical and Physical Data, 97th ed., CRC Press, Taylor & Francis Group, Boca Raton, 2017.
[68] Y. Marcus, Thermodynamics of solvation of ions. Part 5.—Gibbs free energy of hydration at 298.15 K, J. Chem. Soc., Faraday Trans. 87 (18) (Jan. 1991) 2995–2999, https://doi.org/10.1039/FT9918702995.
[69] L. Pauling, The sizes of ions and the structure of ionic crystals, J. Am. Chem. Soc. 49 (3) (Mar. 1927) 765–790, https://doi.org/10.1021/ja01402a019.
[70] L.A. Richards, A.I. Schäfer, B.S. Richards, B. Corry, The importance of dehydration in determining ion transport in narrow pores, Small 8 (11) (Jun. 2012) 1701–1709, https://doi.org/10.1002/SMLL.201102056.
[71] L.A. Richards, A.I. Schäfer, B.S. Richards, B. Corry, Quantifying barriers to monovalent anion transport in narrow non-polar pores, Phys. Chem. Chem. Phys. 14 (33) (Sep. 2012) 11633–11638, https://doi.org/10.1039/C2CP41641G.
[72] R. Epsztein, E. Shaulsky, M. Qin, M. Elimelech, Activation behavior for ion permeation in ion-exchange membranes: role of ion dehydration in selective transport, J. Membr. Sci. 580 (Jun. 2019) 316–326, https://doi.org/10.1016/j.memsci.2019.02.009.
[73] E. Dražević, K. Košutić, V. Freger, Permeability and selectivity of reverse osmosis membranes: correlation to swelling revisited, Water Res. 49 (Feb. 2014) 444–452, https://doi.org/10.1016/j.watres.2013.10.029.
[74] D. Mackay, The tortuosity factor of a water-swollen membrane, J. Phys. Chem. 64 (11) (Nov. 1960) 1718–1719, https://doi.org/10.1021/j100840a026.
[75] J. Kamcev, D.R. Paul, G.S. Manning, B.D. Freeman, Predicting salt permeability coefficients in highly swollen, highly charged ion exchange membranes, ACS Appl. Mater. Interfaces 9 (4) (Feb. 2017) 4044–4056, https://doi.org/10.1021/acsami.6b14902.
[76] T. Rijnaarts, E. Huerta, W. van Baak, K. Nijmeijer, Effect of divalent cations on RED performance and cation exchange membrane selection to enhance power densities, Environ. Sci. Technol. 51 (21) (Nov. 2017) 13028–13035, https://doi.org/10.1021/acs.est.7b03858.
[77] J.H. Choi, J.S. Park, S.H. Moon, Direct measurement of concentration distribution within the boundary layer of an ion-exchange membrane, J. Colloid Interface Sci. 251 (2) (2002) 311–317, https://doi.org/10.1006/jcis.2002.8407.
[78] F.G. Donnan, The theory of membrane equilibria, Chem. Rev. 1 (1) (Apr. 1924) 73–90, https://doi.org/10.1021/cr60001a003.
[79] A.J. Bard, L.R. Faulkner, Electrochemical Methods: Fundamentals and Applications, second ed., John Wiley & Sons, 2001.